Theoretical study of the structures and electronic properties of all-surface KI and CsI nanocrystals encapsulated in single walled carbon nanotubes

Elena Bichoutskaia[1,a] and Nicholas C. Pyper[2]
[1]*Department of Chemistry, University of Nottingham, University Park, Nottingham NG7 2RD, United Kingdom*
[2]*University Chemical Laboratory, Lensfield Road, Cambridge CB2 1EW, United Kingdom*

(Received 4 June 2008; accepted 20 August 2008; published online 15 October 2008)

The structural and electronic properties of all-surface KI and CsI crystals encapsulated in single-walled carbon nanotubes are investigated theoretically with an ionic and atomistic approach using the GULP program. The short-range interactions, derived from Dirac–Fock wavefunctions, were augmented with damped dipole-dipole and dipole-quadrupole dispersive attractions. The uncorrelated interionic interactions computed using the relativistic crystal ion and relativistic integral programs accounted for anion in-crystal modifications while being exact given the ion wavefunctions. All the short-range correlation energies and the uncorrelated interactions between the ions and carbon atoms were computed using the density functional theory of a uniform electron gas of infinite extent. Unphysical self-interactions were removed by scaling the exchange interaction with a Rae factor derived from a study of the adsorption of noble gases on graphite. The predictions for the nonencapsulated crystals agreed well with those previously derived from a global analytic theory based on the Born model. This provided a good description of the contraction of the interplane distance (b) relative to the separation (R_e) in the rocksalt structured bulk material although failing to account for the observed dilation of the intraplane ionic separations (a). Introduction of the interactions with the nanotube wall, including the ion-nanotube dispersive attractions, increased the predicted a values although these were still significantly smaller than experiment. The predicted b separations were reduced compared with those for the nonencapsulated crystals to values significantly less than observed. It is explained why introducing any ion-nanotube interactions that are sufficiently attractive as to reproduce the experimental a values must significantly underestimate the b separations. The partial transfer of anion electrons to the nanotube carbon atoms, not considered hitherto, was described by decomposing the intra-atomic interactions of both the nanotube π- and the iodide $5p$-electrons into an effective one-electron term plus the repulsion between electrons in the same orbital. These energies were derived from electronic structure computations with the additional interspecies electrostatic repulsions derived from the GULP program. Structural predictions are presented as a function of the number (n) of electrons transferred from each anion. For both KI and CsI, the structure predicted by that computation, which minimized the total energy, in contrast to the other calculations, agreed well with experiment reproducing both the significant dilation of a and the smaller contraction of b. The respective n values (n_t) predicting the lowest energies are 0.278 and 0.285. These results are supported by comparing the experimental frequencies of Raman modes attributable to vibrations of nanotubes encapsulating KI with the corresponding frequencies for systems where independently known numbers of electrons were transferred to the nanotubes. In both the encapsulated KI and CsI systems, the charge transfer is driven by the reduction of the electron repulsion on delocalizing some anion charge over the significantly greater number of nanotube carbon atoms. A simplified analytic model, which reproduces the charge transfers, explains why n_t is slighter larger for CsI and also predicts that n_t will be insensitive to the structure of the nanotube. © *2008 American Institute of Physics*. [DOI: 10.1063/1.2987703]

I. INTRODUCTION

Carbon nanotubes have structures that provide excellent templates for assembling low dimensional crystals having controlled architectures on the atomic level. As carbon nanotubes form well-defined cylindrical cavities within a limited diameter range, typically between 10 and 20 Å, their internal van der Waals surfaces regulate the growth behavior of encapsulated crystals, and nanocrystals with precise integral layer architectures can be formed within them. In most cases, structural properties of such crystals are related to the struc-

[a]Author to whom correspondence should be addressed. Tel.: 044-115-9514191. FAX: 044-115-951-3555. Electronic mail: elena.bichoutskaia@nottingham.ac.uk.

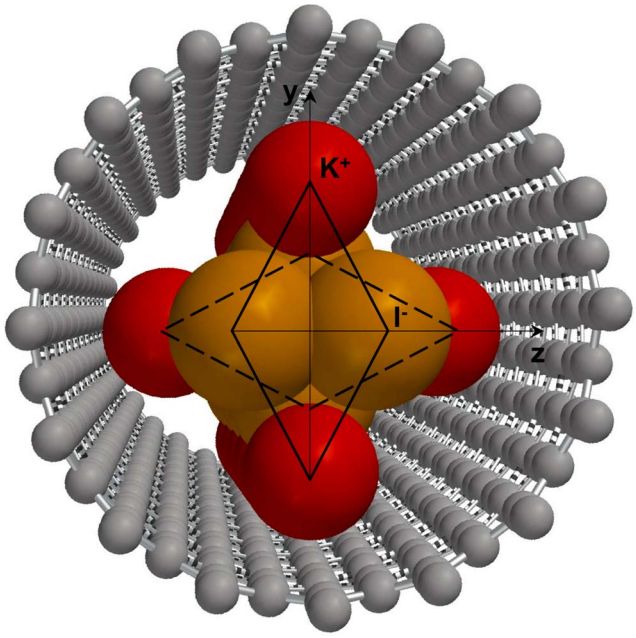

FIG. 1. (Color online) An all-surface KI crystal containing four ions in cross section encapsulated within a (16,0) single-walled carbon nanotube: two potassium ions, K^+ (red) and two iodine ions, I^- (yellow) form (2×2) diamond arrangements in the (y,z) plane which are repeated along the axis of nanotube with adjacent diamonds rotated by 90°. The cation-cation separation $2(K^+)_y$ increases and the anion-anion separation $2(I^-)_z$ decreases with increasing the charge transfer from the anions to the wall.

ture of the bulk material. However, in few instances, crystals with completely new structures are formed inside the nanotubes. One of the more interesting effects of confining crystals within the ultrathin capillaries of carbon nanotubes is the production of structures with reduced or modified coordination that also exhibit significant structural distortions when compared to the bulk materials.

For alkali halides, such confinement can result in the formation of all-surface crystals with as few as two atomic layers in cross section and no internal atoms (Fig. 1). The first such material prepared was an all-surface KI crystal with (2×2) atoms in cross section confined within a single walled carbon nanotube (SWNT).[1] Its high-resolution transmission electron microscope (HRTEM) image shows, along the nanotube axis, an array of pairs of identical dark spots representing alternating columns of I–K and K–I viewed in projection. It was deduced from these observations that the encapsulated nanocrystal consists of a succession of planes, each containing four ions, orientated perpendicular to the nanotube and so that each ion has closest neighbors of only the opposite charge. In this nanocrystal, derived from a small piece of the bulk rocksalt lattice, all ions undergo a reduction from sixfold to fourfold coordination which causes significant distortions of the structure from the rocksalt bulk material. The experimental measurements[1] indicate that the in-plane K–I separation (a) across the SWNT is on average 3.98 ± 0.31 Å representing a 12% expansion from the 3.52 Å closest cation-anion separation (R_e) in the rocksalt structured bulk material.[2] By contrast, the separation (b) between the K^+ and I^- ions along the SWNT axis, that is, the, interplane distance, is slightly reduced from the bulk spacing to the average value of 3.46 ± 0.03 Å. For all of the iodides from Li to Rb, the predominant structure observed by HRTEM inside SWNTs has been the rocksalt form. Only CsI forms significant quantities of *bcc*-type halide inside the SWNT; however, the more usual structure for this halide remains $(2\times2\times\infty)$ rocksalt-type crystal. The rocksalt $(2\times2\times\infty)$ CsI crystal encapsulated within a SWNT also exhibits structural distortions as manifested by a 7% expansion of the a distance coupled with 3% contraction in the b separation when compared with 3.81 Å spacing[3] in bulk rocksalt structured CsI. Thus, the separations in the encapsulated CsI were found to be $a=4.1\pm0.2$ Å and $b=3.7\pm0.2$ Å.[4]

Previously, there have been a few attempts made to explain the factors governing structural lattice distortions of the encapsulated alkali halide crystals. Molecular dynamics simulations based on atomistic models[5,6] have been used both to suggest possible mechanisms for the growth of KI crystals in carbon nanotubes and to interpret the results of HRTEM experiments.[1] These simulations explained how the nanotubes were filled through immersion in liquid KI. The a/b ratio calculated for the $(2\times2\times\infty)$ KI crystal only agreed with the experimental value if the nanotube in the simulation was taken to be immersed in molten KI. However, there was no molten salt surrounding the nanotube during the HRTEM experiments from which the structure was deduced. It was further shown experimentally that the structures of the encapsulated salts remained unchanged on annealing a filled nanotube.[7] The density functional theory (DFT) linear augmented plane wave (LAPW) computations[8] for $(2\times2\times\infty)$ KI using the muffin-tin approximation and assuming the experimentally observed nuclear positions probed just the electronic charge distribution. Another DFT study[9] of the structure of this system, although reproducing the experimental value of the b distance, does not predict the dilation of a, which was computed to be 3.49 Å compared with the experimental 3.98 Å.

In this paper, the first comparative study of the structures of two encapsulated nanocrystals, $(2\times2\times\infty)$ KI and $(2\times2\times\infty)$ CsI, is presented by first giving predictions for nonencapsulated crystals and then introducing three types of ion-wall interactions in which the species become increasingly interconnected. The methodology adopted here is to systematically but separately elucidate each of the interactions and different physical effects which are then combined in a full description of the system of nanotube plus encapsulated nanocrystal. This approach not only provides physical insight into the factors determining the structures and reveals the relative importance of each factor but also opens up the possibility of subsequently refining the description of those effects, which have been found to be significant. Here we show that the structures determined in the HRTEM experiments can be explained and reproduced only with the inclusion of, first, the dispersive attractions between both the ions and the ions and nanotube wall, second, a physically soundly based description of the short-range repulsion between the ions and wall, as well as, third, allowing for crystal to wall charge transfer.

TABLE I. Ion dependent variables needed to calculate the dispersion attractions (a.u.). Free cation α_C, $\langle r^2\rangle_C$ and $\langle r^4\rangle_C$ from Refs. 13 and 15. α_A from Ref. 15 by subtracting α_C from the experimental molar polarizability from Ref. 43. d_C derived (Refs. 13 and 15) from orbital eigenvalues according to theory of Refs. 10 and 28. d_A from Ref. 15 derived from spatial decay of the outermost orbitals according to theory of Ref. 11. Anion electronic expectation values from Ref. 15.

	α_C	α_A	P_C	P_A	$\langle r^2\rangle_C$	$\langle r^4\rangle_C$	$\langle r^2\rangle_A$	$\langle r^4\rangle_A$	d_C	d_A
KI	5.339	44.869	6.106	7.901	14.479	62.230	46.581	599.491	2.423	1.445
CsI	15.28	46.602	7.901	7.901	29.438	226.535	47.135	613.732	2.130	1.507

II. METHODOLOGY

A. Total crystal energy and structure

The system of ions plus nanotube is treated as a collection of mononuclear species interacting mainly through two-body interactions depending only on internuclear separations. Although, for no crystal to wall charge transfer, many of the methods[10–14] and some potentials[15] have been reported, a summary is needed. The intraionic interactions derived using an ionic description, supported for alkali halides by extensive evidence,[16,17] provide an excellent description of the structures and energetics of nonencapsulated bulk crystals.[10–13,18–21] The present atomistic methods also describe[14] the adsorption of noble-gas atoms on graphite as acceptably as the computations[22] in which standard DFT was augmented with semiempirically determined terms describing the dispersive attractions. In contrast to the present approach, computational limitations restricted the DFT investigation to the lightest noble gases. The atomistic methods enable the structures of the nanocrystals to be predicted using the GULP program,[23] which yields the total energy of a system of interacting mononuclear species expressed relative to the sum of their isolated energies. This program both allows ion-induced dipole interactions to be investigated and enables each carbon atom permanent electric quadrupole moment,[24,25] generated by the π-electron charge concentrated around the nanotube, to be modeled as three point charges.

Cations and anions carrying their formal charges are denoted by C and A with X and Y denoting any ion. Carbon atoms of the nanotube wall are labeled W with G and H denoting any species. The geometry of a crystal interacting with a nanotube is predicted by minimizing the energy $U(\boldsymbol{r}_X)$ with respect to the ion coordinates denoted by $\boldsymbol{r}_X$. In the absence of transfer of charge between the crystal and tube, one has

$$U(\boldsymbol{r}_X) = U^{\mathrm{el}}(\boldsymbol{r}_X) + U^{\mathrm{IID}}(\boldsymbol{r}_G) + \sum_{G<H} V_{GH}(r_{GH}). \tag{2.1}$$

Here $U^{\mathrm{el}}(\boldsymbol{r}_X)$ is the total electrostatic energy treating each species as a point carrying its formal charge or, when including carbon quadrupole moments, the interactions of all charges except those within a single quadrupole. The ion-induced dipole energy $U^{\mathrm{IID}}(\boldsymbol{r}_G)$ is not included in $U^{\mathrm{el}}(\boldsymbol{r}_X)$ but is described using the shell model[26] where each species is defined by a nonpolarizable core which binds a shell through a harmonic potential. Since the shell positions are chosen to minimize the total energy, ion-induced dipole energies yielded by the GULP program depend only on the nuclear coordinates.

Each $V_{GH}(r_{GH})$ in Eq. (2.1) yields the interaction of species G and H separated by a distance r_{GH} after subtracting any point Coulombic energy equal to the product of the formal charges of G and H divided by r_{GH}. This potential is composed of the contribution $V^0_{sGH}(r)$ that would arise in the absence of electron correlation plus two correlation terms $V^{\mathrm{corr}}_{sGH}(r)$ and $V^{\mathrm{disp}}_{GH}(r)$, as justified in the review[16] and confirmed by the investigation[27] of the noble-gas dimers which provide a severe test of any theory. Thus,

$$V_{GH}(r) = V^0_{sGH}(r) + V^{\mathrm{corr}}_{sGH}(r) + V^{\mathrm{disp}}_{GH}(r). \tag{2.2}$$

The subscript s denotes that $V^0_{sGH}(r)$ and $V^{\mathrm{corr}}_{sGH}(r)$ are of short range, depending explicitly on the overlap of the electron densities of G and H, and vanish for large r where this overlap is negligible. The dispersive attraction $V^{\mathrm{disp}}_{GH}(r)$ is of long range in that it does not vanish for those r at which the overlap has become negligible but has there a leading term varying as r^{-6}.

B. Components of the total energy

1. The dispersive attractions

Each $V^{\mathrm{disp}}_{GH}(r)$ was evaluated as the sum of the dipole-dipole and dipole-quadrupole terms, damped at short r where wavefunction overlap is not negligible, by an r dependent function determined by damping parameters d_G and d_H (Tables I and II). The damping functions[10,11,28] are assembled elsewhere.[27]

The $C_6(GH)$ coefficients were calculated via the Slater–Kirkwood formula[29] from the polarizabilities (α_G) and electron numbers (P_G). The $C_6(XY)$ coefficients were derived[15] from the data in Table I using free ion α_C because there is extensive evidence[10,17,30–34] that the properties of cations having p^6 outermost electronic configurations are essentially

TABLE II. Parameters determining the ion-wall carbon dispersive attractions (a.u.). Electronic expectation values computed from the carbon wavefunction described in Ref. 14. d_W derived from the relation (5) of Ref. 14 provided by the Lassettre theory (Ref. 85) using experimental data for a free carbon atom.

	$C_6(CW)$	$C_8^{\mathrm{DQ}}(CW)$	$C_8^{\mathrm{QD}}(CW)$	$C_6(AW)$	$C_8^{\mathrm{DQ}}(AW)$	$C_8^{\mathrm{QD}}(AW)$	$\langle r^2\rangle_W$	$\langle r^4\rangle_W$	d_W
KI	20.730	280.954	133.645	127.583	1729.14	2462.96	3.890	35.143	1.437
CsI	53.203	721.062	614.121	131.404	1780.92	2566.46	3.890	35.143	1.437

unaffected by their environment in crystal. The derivation of each P_X from data for the isoelectronic noble gas should ensure that the $C_6(XY)$ coefficients are correct to within 5%.[10,31] The $C_6(XW)$ coefficients (Table II) were calculated using the 10.26 a.u. mean carbon polarizability derived[14] from the atomic polarizabilities, parallel and perpendicular to graphene sheets, of 13.46 and 3.85 a.u., deduced from experimental studies of the dielectric properties of graphite and a semiempirical analysis of its measured compressibility.[35,36] The 1.118 value of P_W, ensuring[14] that the Slater–Kirkwood formula reproduced the $C_6(GW)$ derived[37] from an analysis of experimental data for the xenon-graphite interaction, is consistent with the idea that the polarizability of graphite originates mainly from the π-electrons. Justification is presented elsewhere.[14]

The dipole-quadrupole dispersion coefficients were computed from the $C_6(GH)$ coefficients by using the Starkschall–Gordon formula.[38] The expectation values (Table II) for the outermost electrons were derived, as justified,[10,39] from free cation and free carbon atom wavefunctions but with anion functions computed for the equilibrium geometry of the bulk rocksalt structured crystal taking account of the in-crystal induced modifications[10,11,15] of the anion properties. The introduction of scaling factors into the calculation of the purely intracrystal coefficients ensures that these are correct to within 5%.[12]

The description of dispersive attractions to a semiconducting nanotube by atomistic methods might appear questionable. However, London commented[40] that the behavior of species in rapidly time varying fields, such as those responsible for dispersion forces, tends to that of a collection of its individual atoms. Thus it is interesting that accurate *ab initio* electronic structure computations[41] show that the average polarizability of a free carbon atom is 11.83 a.u., similar to that of an atom in graphite.

2. Induced dipole and permanent quadrupole interactions

The shell model description of $U^{\mathrm{IID}}(\mathbf{r}_G)$ requires shell charges q_G and spring constants k_G yielding α_G as q_G^2/k_G.[26] The natural choice, P_G, was made for the magnitude of the (negative) cation and carbon q_G, with k_C derived from α_C. Since dipoles induced on the nanotube would, on average, be expected to be perpendicular to its axis, the component perpendicular to the graphene sheet of the polarizability of such a carbon atom was used to derive k_W. Since the α_A are significantly affected by the in-crystal environment, the q_A and k_A in KI of −2.515 and 0.12537 a.u. were derived, as for RbCl,[19] by demanding that the experimental values of 5.6 for static dielectric constant[42] and 50.208 a.u. for the high frequency crystal molar polarizability extrapolated to infinite wavelength[43] were reproduced. The q_A magnitude, although smaller than P_A, is not dissimilar to either that of 3.4 a.u., similarly found[19] for RbCl, or that of 3.0 a.u. deduced using semiempirical potentials for the anion in the alkali iodides.[44]

Each carbon quadrupole moment was modeled by locating a 1 a.u. charge at the carbon nucleus with two negative charges of magnitude 0.5 a.u. placed inside and outside the nanotube at a distance of 1.039 a.u. with the line of three charges perpendicular to the nanotube axis. This reproduces the −1.08 a.u. zz quadrupole component used in the study[14] of the adsorption of noble gases on graphite.

3. Short-range correlation and intracrystal interactions

The short range interactions in Eq. (2.2) were computed from relativistic Dirac–Fock wavefunctions for isolated cations and carbon atoms. The anion functions were computed using the RIP/RELCRION (Refs. 19 and 45) program with the optimized hyperbolic secant Madelung–Fermi-smoothed (OHSMFS) model Hamiltonian taking account of their important modifications caused by the in-crystal environment.

The latter computations, performed for the rocksalt structured bulk crystal over a range of closest cation-anion separations, yielded uncorrelated cation-anion $V^0_{sCA}(r_{CA})$, anion-anion $V^0_{sAA}(r_{AA})$, and cation-cation $V^0_{sCC}(r_{CC})$ potentials[15] which are exact given the wavefunctions of the two species. Use of the OHSMFS model introduces into the total crystal energy, the rearrangement energy needed to convert a free anion into its form optimal for the crystal having the considered geometry. Since the GULP program cannot handle rearrangement energies, $V^0_{sCA}(r_{CA})$ and $V^{\mathrm{corr}}_{sCA}(r_{CA})$ were effective potentials[46] consisting of the two-body potential computed using the RIP program plus one-sixth of the rearrangement energy.

For all pairs, $V^{\mathrm{corr}}_{sGH}(r)$ was evaluated as the difference between the correlation energies of the interacting and noninteracting species using the local DFT of a uniform electron gas with the electron density in the interacting pair taken to be the sum of those of the noninteracting species, the Gordon–Kim method.[47] The correlation contribution to the rearrangement energy needed to calculate the $V^{\mathrm{corr}}_{sCA}(r_{CA})$ was derived[15] by scaling[12] the prediction of local uniform electron-gas DFT introducing the Cowan modification[48] which eliminates terms describing the interaction of each electron with itself.

4. The uncorrelated short-range ion-nanotube interactions

The computation of the uncorrelated short-range repulsions $V^0_{sXW}(r)$ between the ions and wall carbon atoms merits a fuller discussion because its physics will be seen to raise important issues. The DFT of a uniform electron gas was taken as the basis for computing these repulsions. In the approach used here, introduced by Massey and Sida,[49] the electron density of the interacting pair is taken to be the sum of the Hartree–Fock densities of the individual mononuclear species and $V^0_{sGH}(r)$, composed of three distinct contributions, is evaluated as the difference between the energies of the interacting and noninteracting species. The first contribution to $V^0_{sGH}(r)$, the nonpoint Coulomb term, is the purely electrostatic interaction that would arise in the absence of interatomic electron exchange. This contribution, calculated exactly, is that remaining after subtracting the point Coulombic term equal to the product of the net charges of species G and H divided by their internuclear separation. The two remaining contributions to $V^0_{sGH}(r)$, those arising from the kinetic and exchange energies of the electrons, are calculated

using the functionals for a uniform electron gas of infinite extent. However, it has been shown[50,51] that this method of calculating $V^0_{sGH}(r)$ significantly underestimates the repulsion between two closed shell atoms or ions because the negative contribution arising from electron exchange, being computed from the functional derived for an electron gas of infinite extent, is too large in magnitude. The functional derived under these two assumptions includes the nonexistent exchange of an electron with itself, a contribution which is only a negligible fraction of the total exchange for a system of infinite extent. For a system of finite extent, it was shown[50,51] that this unwanted self-exchange could be eliminated by multiplying the exchange energy by a correction factor $\gamma(N)$ depending on the effective number (N) of electrons contributing to the interatomic interaction. It was further shown[52–54] that, for the interaction of two mononuclear species, the effective number N should be taken to be the total number of outermost electrons on both species, this being 16 for the interaction of two mononuclear species of s^2p^6 outermost electronic configurations.

In the computation of the exchange interaction between an isolated carbon atom and an ion of s^2p^6 outermost electronic configuration, the appropriate N value would clearly lie in the range between 9 and 12. However, it has to be questioned whether an N value in this range would be right for treating the interaction between an ion and a carbon atom belonging to a semiconducting or metallic nanotube of infinite extent in one dimension. Insight into this issue has been provided by an investigation[14] of the adsorption of a single Ar, Kr, or Xe atom onto the surface of a graphene sheet. Each two-body noble-gas–carbon interaction was calculated through the relation (2.2) using the same methods as those used here including both the short-range interactions and the dispersive attractions. It was found that the binding was seriously underestimated, as manifested by too small cohesive energies and too large equilibrium noble-gas–graphene distances if N was taken to lie in the 9–12 range. However, these deficiencies were rectified for all three gas-graphene systems by using the same larger N of 500 corresponding to a $\gamma(500)$ value of 0.79484, compared with $\gamma(12)=0.35153$. It should be emphasized that the derivation of this result has not involved invoking any experimental data for the nanotube systems but has been deduced by examining closely related systems that are not the objective of the present study. Furthermore, there are good theoretical reasons[14] for expecting that the N values for interactions with a spatially extended semiconducting material will be much larger than those appropriate for the interaction of just two atoms. All the present results were computed from the wavefunctions already described using this 500 value for N.

C. Anion-wall charge transfer

The possibility of anion to wall charge transfer, that is, the partial transfer of anion electrons to the wall carbon atoms, can be investigated by combining the ideas used in Ref. 55 to explain the observed regularities between successive atomic ionization potentials with some concepts from DFT.[56] It is consistent with the latter to introduce a continuous and fractional number of electrons (n) transferred from each anion to the wall carbon, each of which acquires a charge $(-nf)$, where there are f^{-1} carbon per anion. For each anion and each carbon, the total energy of the outermost electrons is decomposed into the contributions from the negative effective one-electron energies, denoted I^{ne}_A and I_W for anion and carbon, respectively, plus the total intra-atomic repulsion between these outermost electrons. For mononuclear species G, the effective one-electron energy (I_G) is the sum of the kinetic energy and nuclear attraction of a single electron in the outermost orbital of species G plus the repulsion of this electron with all other electrons belonging to G except those in the same outermost orbital. For an I^- ion in a relativistic description, there are four outermost electrons, namely, the $5p$-electrons each having a total angular momentum $j=3/2$. Each of these lies some 0.0395 a.u. higher in energy than each of the $5p$-electrons having $j=1/2$. The additional superscript "ne" (standing for "no environment") on I^{ne}_A denotes that this energy is purely intra-atomic and does not include the interaction of the anion electron with any other ions in the crystal. In the absence of charge transfer, each carbon is considered to have one outermost electron, that in the orbital which is approximately perpendicular to the nanotube wall. The intra-atomic repulsions between, respectively, a single pair of anion $5p$-electrons and a single pair of outermost carbon electrons in the $2p_z$ orbital are denoted F_A and F_W. After transfer of n electrons per anion, there are $(1+nf)$ outermost electrons on each carbon thus leaving each anion with $4-n$ outermost electrons. The sum $E^{\mathrm{OC}}(n)$ per anion of all these purely one-centered (OC) electronic energies is given by

$$E^{\mathrm{OC}}(n) = (4-n)I^{\mathrm{ne}}_A + (1/2)(4-n)(3-n)F_A + f^{-1}[(1+nf)I_W + (1/2)(1+nf)nfF_W], \quad (2.3)$$

with the electron repulsion term for each species G having m_G outermost electrons being expressed as $(1/2)m_G(m_G-1)F_G$. The difference $\Delta E^{\mathrm{OC}}(n)$ between Eq. (2.3) and the one-center energy $[E^{\mathrm{OC}}(0)]$ arising in the case of no electron transfer $(n=0)$ is given by

$$\Delta E^{\mathrm{OC}}(n) = E^{\mathrm{OC}}(n) - E^{\mathrm{OC}}(0). \quad (2.4)$$

The energies I_W and F_W were evaluated for an sp^2p_z state of the carbon atom by combining the results of an *ab initio* computation with an analysis of experimental data. This procedure is described in detail in the Appendix. The anion energies I^{ne}_A and F_A were obtained directly from the RIP/RELCRION computations of the cohesive properties of the bulk crystals.[15] For KI and CsI these were taken from the computations performed for the respective bulk separations of 7.0 and 7.375 a.u., these values being close to the average of the experimentally observed a and b values of 3.98 and 3.46 Å for KI (Ref. 1) and 4.1 and 3.7 Å for CsI.[4] For distances close to the experimental separations in either the bulk materials or those in the nanocrystals, both I^{ne}_A and F_A depend only weakly on distance, the major distance dependence of the charge transfer energy at constant n arising from the multicenter interactions described in the next paragraph.

There are four effects arising from the partial ionization of all the anions which involve changes in the interactions between pairs of species and which therefore depend on n. The first three of these, the attraction to the positively charged crystal of the electrons transferred to the wall, the mutual repulsion between these wall electrons on different atoms, and the reduction of the Madelung energy of the encapsulated crystal, are automatically included when the energy, denoted $U^{\mathrm{GULP}}(\boldsymbol{r}_X;n)$, of the system of crystal plus encapsulating nanotube is computed using the GULP program. Such a computation differs from that yielding Eq. (2.1) only in that the magnitude of the anion charge is reduced to $(1-n)$ with each carbon atom acquiring a net charge of $-nf$. The fourth interspecies effect arising from the transfer of n electrons from each anion is the energy lowering resulting from the removal of that part of the density of these electrons from spatial regions of non-negligible cation electron density. This energy is automatically obtained as a by-product of the computation of the anion wavefunction using the OHSMFS model Hamiltonian[11] for the interaction of an anion electron with the in-crystal environment generated by the other ions.

The OHSMFS Hamiltonian is the sum of two terms. The first of these describes the electrostatic potential generated by all the remaining ions in the crystal while the second, originating ultimately from the Pauli principle, is the repulsion experienced by an anion electron in those regions of space in which the electron densities of neighboring ions are not negligible. Although an anion electron transferred to the nanotube wall ceases to experience the first contribution to the OHSMFS potential, this effect is automatically included in the energy $U^{\mathrm{GULP}}(\boldsymbol{r}_X;n)$. For one single anion $5p$-electron at a distance r_a from its nucleus, the repulsive energy, denoted I_A^{ov}, generated by the overlap of its electron density with that generated by one cation located at a distance R is given by the expectation value of the second term in the OHSMFS environmental potential

$$I_A^{\mathrm{ov}} = \langle 5p|A\ \mathrm{sech}[k(r_a - R)]|5p\rangle/6. \tag{2.5}$$

The values of the variationally determined parameters A and k were computed[15] for an anion in the rocksalt structured bulk material. The factor of 6 arises because one anion electron experiences an energy of $6I_A^{\mathrm{ov}}$ in the rocksalt structured bulk crystal. Since each anion in the nanocrystal has four cation neighbors, the loss of this overlap repulsion on the transfer of n anion electrons introduces a contribution $-4nI_A^{\mathrm{ov}}$ to the total energy. For each salt, the expectation value in Eq. (2.5) was computed for the structure having the internuclear separation R specified in the last paragraph.

The total energy $U_T(\boldsymbol{r}_X;n)$ of the entire system of nanocrystal plus encapsulating nanotube, expressed on the same scale as that used in Eq. (2.1), is therefore given by the sum of the interspecies interaction energy $U^{\mathrm{GULP}}(\boldsymbol{r}_X;n)$ plus the purely one centered energy $\Delta E^{\mathrm{OC}}(n)$ arising from charge transfer augmented with the reduction of $4nI_A^{\mathrm{ov}}$ in the overlap repulsion. The result is

$$U_T(\boldsymbol{r}_X;n) = U^{\mathrm{GULP}}(\boldsymbol{r}_X;n) - 4nI_A^{\mathrm{ov}} + \Delta E^{\mathrm{OC}}(n). \tag{2.6}$$

The energy $U_T(\boldsymbol{r}_X;n)$ is expressed like Eq. (2.1), with respect to the sum of the energy of the isolated nanotube plus free ions carrying their formal charges. Thus, in the $n=0$ limit, Eq. (2.6) reduces to the no charge transfer result (2.1). For fixed n, the optimal structure, which minimizes $U_T(\boldsymbol{r}_X;n)$, is given by

$$[dU_T(\boldsymbol{r}_X;n)/d\boldsymbol{r}_X]_{\boldsymbol{r}_X=\boldsymbol{r}_{X_e}} = 0 = [dU^{\mathrm{GULP}}(\boldsymbol{r}_X;n)/d\boldsymbol{r}_X]_{\boldsymbol{r}_X=\boldsymbol{r}_{X_e}}, \tag{2.7}$$

with the second result obtained by using the good approximation that $\Delta E^{\mathrm{OC}}(n)$ and I_A^{ov} are independent of the $\boldsymbol{r}_X$. The resulting total minimum energy, $[U_T(\boldsymbol{r}_X;n)]_{\boldsymbol{r}_X=\boldsymbol{r}_{X_e}}$, being no longer a function of $\boldsymbol{r}_X$, can be expressed as

$$[U_T(\boldsymbol{r}_X;n)]_{\boldsymbol{r}_X=\boldsymbol{r}_{X_e}} = U_{T_e}(n). \tag{2.8}$$

The result (2.6) is expected to capture the essential physics of the charge transfer process because it includes the changes introduced into the dominant interactions, namely, the purely one-center energies and the Coulomb terms. Since the contributions of the nonpoint Coulombic interactions $V_{XY}(r_{XY})$ are only some 10% of the total binding in the bulk crystal, effects arising from any charge transfer induced changes in the two-body potentials in Eq.(2.1) would be expected to be small. Hence a detailed investigation of these effects lies outside the scope of the present study although they are partially included via the $-4I_A^{\mathrm{ov}}$ term in Eq. (2.6). The optimum structure, which has the lowest energy overall, is that having the n value, denoted n_t, minimizing $U_{T_e}(n)$ so that

$$[dU_{T_e}(n)/dn]_{n=n_t} = 0. \tag{2.9}$$

Thus, under assumption that the purely one centered energy $\Delta E^{\mathrm{OC}}(n)$ is independent of structure, there is an optimal structure of energy $U_{T_e}(n)$ for every fixed n, so that Eq. (2.9) expresses the result that the structure having the lowest energy overall must be that of lowest energy amongst those having energies $U_{T_e}(n)$.

III. RESULTS AND DISCUSSION

A. Nonencapsulated crystals

For nonencapsulated nanocrystalline ionic solids, a recently presented analytic theory[57] based on the Born model was shown to be capable of explaining both their structures and energetics on a global and unified basis. This approach is based on the assumption that the crystals are fully ionic and focuses only on the largest and most important terms, namely, the Coulombic interactions between the ions treated as point charges and the short-range repulsive interactions between immediately neighboring ions. It exposes the relationship between the nanocrystals and the bulk rocksalt phases and shows how structural properties of the nanocrystals evolve toward those of the bulk as the number of atoms in the planes is increased. In particular, for the low dimensional crystals, this model predicts contractions of the b distance relative to the bulk separations R_e and ratios b/R_e in good agreement with the experimental results for the encap-

TABLE III. Interionic separations (in Å) across (a) and along (b) the crystal chain in bare KI (2×2) and CsI (2×2) nanocrystals as well as encapsulated within a (16,0) SWNT. For encapsulated crystals, the calculated results are shown without a charge transfer from the anions onto the wall of nanotube ($n_t=0$) and with the optimal charge transfer predicted by minimizing the total energy including charge transfer, as described in the text.

	KI			CsI		
	n_t	a	b	n_t	a	b
Bare crystal/Born model[a]	···	3.46	3.38	···	3.74	3.67
Bare crystal/GULP	···	3.43	3.37	···	3.73	3.71
Crystal @ (16,0) SWNT (no charge transfer)	0	3.66	3.31	0	3.92	3.50
Crystal @ (16,0) SWNT (charge transfer)	0.278	3.97	3.54	0.285	4.04	3.73
Crystal @ (16,0) SWNT, (experiment)	···	3.98[b]	3.46[b]	···	4.10[d]	3.70[d]
Rocksalt bulk experiment	···	3.52[c]	3.52[c]	···	3.81[e]	3.81[e]

[a]Reference 57.
[b]Reference 1.
[c]Reference 2.
[d]Reference 4.
[e]Reference 3.

sulated crystals.[1,4] This contrasts with the result that the a/R_e ratios are found to be less than unity. It also predicts that the a/b ratios are greater than unity. This approach yields predictions, presented in the first line of Table III, for the absolute values of a and b if the experimental values for R_e are combined with these two ratios.

The validity of the above results derived from the analytic model is confirmed here by using more sophisticated nonempirical interionic potentials[13,15] from which the structures of the bare nonencapsulated $(2\times2\times\infty)$ KI and CsI nanocrystals were first computed as described in Secs. II A and II B. The interionic separations a and b predicted from this approach for the $(2\times2\times\infty)$ nanocrystals (see "bare crystal/GULP" results presented in Table III) are in a good agreement with the analytical model[57] ("bare crystal/Born model" results in Table III). Introduction of the shell model to describe ion-induced dipole effects, as described in Sec. II B 2, yielded for KI $a=3.44$ Å and $b=3.38$ Å. The similarity between these predictions and those presented in Table III shows that intracrystal ion-induced dipole effects are so small that they will not be further considered.

B. Encapsulated crystals without charge transfer

1. The purely two-body description

The structural distortions, shown by the results presented in the first two numerical rows of Table III, arise solely from the low dimensionality of the nanocrystal and are not caused by interaction with the wall of encapsulating nanotube. Although the predicted a/b ratios for bare nanocrystals are greater than unity, their values are significantly less than those derived from experiment. This result coupled with the prediction of a/R_e ratios less than 1, not consistent with experiment, shows that interactions with the nanotube wall are important.

The diameter of a SWNT encapsulating the $(2\times2\times\infty)$ KI nanocrystal was reported to be about 14 Å.[1] However, this value was found to be inconsistent with other measurements presented in Fig. 1(a) of Ref. 1. This diameter was later remeasured as 12.8 Å. Since the chirality of the encapsulating nanotube is not available from experiment, we considered the crystal to be encapsulated in a zigzag (16,0) nanotube, because zigzag nanotubes have the smallest repeat distances while the 12.5 Å diameter of a (16,0) nanotube is close to the experimental value. The diameter of the nanotube encapsulating the $(2\times2\times\infty)$ CsI nanocrystal was the same as that in the $(2\times2\times\infty)$ KI system.

The first of the three types of ion-wall interaction consists of the totality of all the ion-carbon pair potentials $V_{XW}(r)$ (2.2). For both of the encapsulated crystals, the results, calculated after introducing these terms and taking N to be 500 in the computation of the uncorrelated short-range repulsions $V^0_{sXW}(r)$, are presented in the third numerical row of Table III. Comparison of these results with those of bare nanocrystal shows that introducing the interactions with the wall predicts the a separations to be greater than in the bulk, in agreement with experiment. However, the predictions for a values remain appreciably smaller than the experimental values in the nanocrystal, while the b separations are now significantly underestimated compared with both the experiments and the calculations for the bare nanocrystals. It is of interest to note that use of the more repulsive ion-wall interactions generated by taking N to be 12, although rectifying the underestimation of the b spacing, still fails to predict the dilation of the a spacing. Thus the results of $a=3.48$ Å, $b=3.35$ Å for KI obtained when N is taken to be 12 are not very different from those predicted for the bare nanocrystals. The appreciable change in the predictions produced by taking N to be 12, rather than the 500 value deduced from the study[14] of the adsorption of noble gases on graphite, shows

how significantly the semiconducting property of the nanotube influences the structures of the encapsulated nanocrystals. These variations in the predictions for a and b caused by changing the strength of the ion-carbon short-range repulsions $V^0_{sXW}(r)$ can be understood by the following arguments based on the previous analytic model.[57]

The equilibrium distance b in a nonencapsulated one dimensional single chain is less than that in the rocksalt structured bulk crystal because, on passing from the latter to the former, the attractive Madelung energy is only reduced in magnitude from $1.74756/R$ to $2\ln 2/R$ at constant R (1.74756 is the bulk Madelung constant), while the number of closest short-range cation-anion repulsions is reduced by a factor of 3. On passing from the one dimensional single chain to the nonencapsulated $(2\times 2\times\infty)$ nanocrystal, the number of closest short-range repulsions is doubled, while the additional binding resulting from the electrostatic interactions between two adjacent chains is only $-0.116741/R$ with the interaction between the two chains separated by the distance $a\sqrt{2}$ generating[57] a repulsion of $0.02857/R$. This explains why the equilibrium values of both a and b are larger than those in the one dimensional chain. It then follows that any increase in a from its equilibrium value in the nonencapsulated nanocrystal produces a structure in which reduction of b will cause an enhancement of the electrostatic attraction which is greater than the increase of the purely intracrystal short-range repulsion. This shows that enhancement of a induced by attraction to the nanotube wall will cause the chains to contract along their lengths with the resulting b values tending, in the limit of very large a, toward the b value of the one dimensional single chain. This explains why any calculation based on Eq. (2.1), thus not considering charge transfer, which uses a value for N sufficiently large as to reproduce the experimental a value will inevitably underestimate the b separations.

2. The potential role of higher order multipole moments on wall atoms

The second type of ion-wall interaction consists of those originating from dipole and high order moments, either permanent or induced. These terms were computed using the methods described in Sec. II B 2.

The electric field generated at the nanotube wall as the sum of those originating from the ions of the nanocrystal can, in principle, induce an electric dipole moment on each wall carbon thus contributing to the attraction designated $U^{\mathrm{IID}}(\boldsymbol{r}_G)$ in Eq. (2.1). The resulting predictions of $a=3.66$ Å and $b=3.31$ Å for KI are unchanged from those derived neglecting the ion-wall induced dipole terms.

The π-electron charge in graphite concentrated above and below the graphene sheets causes each carbon atom to possess a permanent electric quadrupole moment of negative sign. Not only is the interaction of these moments a significant factor determining the stacking of graphene sheets in graphite but they also make an important contribution to the adsorption of both water and nitrogen by graphite.[24] Furthermore, ionic species are bound above the rings of aromatic hydrocarbons through the interaction of ion charges with the carbon quadrupoles, the widespread occurrence of such cation-π interactions being reviewed elsewhere.[25] The importance of the carbon quadrupole moments in these three ways shows the need to investigate their potential significance for the nanocrystals encapsulated in carbon nanotubes. However, the introduction of these wall quadrupole moments left the a and b values predicted for the encapsulated KI unchanged at $a=3.66$ Å and $b=3.31$ Å.

The calculations just described show that both the ion-induced carbon dipole terms and the charge permanent quadrupole interactions are unimportant for the encapsulated nanocrystals. This is consistent with the well-established result[58] that the electric field generated by a bulk crystal has become negligible at distances from the crystal surface, which are greater than the lattice spacing. Hence neither of these interactions needs to be further considered.

C. Charge transfer from anions to nanotube wall atoms

1. Multianion description

The third type of crystal-wall interaction, which exhibits the greatest degree of mutual entanglement, is the partial transfer of anion electrons to the nanotube. The possible significance of this process was investigated by predicting the optimal structures and their energies $U_{T_e}(n)$ as a function of the number n of electrons transferred per anion by using the relations (2.6)–(2.9). The actual charge transfers n_t, predicted as the n value yielding the lowest $U_{T_e}(n)$, were found to be 0.278 and 0.285 for KI and CsI, respectively.

The DFT LAPW computation for KI,[8] performed at one nuclear geometry, is in qualitative agreement with our present results that charge is transferred from the anions to the wall, although more detailed analysis shows much transfer to the intersphere regions present in this DFT method. By contrast, the predictions of another DFT computation[9] yielded a charge transfer that was not only small but also in the opposite direction, from the wall to the crystal. The inability of standard DFT to reproduce dispersive attractions coupled with the minimal predicted charge transfer explains why this approach underestimated[9] the a separation by 0.5 Å.

The relation (2.3) shows that the total repulsion between all the outermost electrons on each ion contains a contribution varying quadratically with the numbers of electrons while the total effective one-electron energy is a purely linear function of the number of electrons. For KI and CsI, the respective I_A^{ne} values of -1.08399 and -1.08651 a.u. are both more negative than the effective one-electron energy (I_W) of -0.44109 a.u. for a nanotube π-electron. However, the delocalization over the wall of any charge transferred from each anion causes the intraionic electron repulsion to be lowered to a much greater extent than the repulsion experienced by these transferred electrons when their density is spread over f^{-1} nanotube carbon atoms [f^{-1} being 28 for a (16,0) SWNT]. These observations show that any energy lowering resulting from charge transfer must arise because the reduction of the total electron-electron repulsion through this delocalization must be greater than the increase in the total one-electron energy. This mechanism driving the charge

TABLE IV. Structural changes (in Å) in the KI (2×2) and CsI (2×2) nanocrystals as a function of charge transfer from the anions onto the wall of the (16,0) SWNT.

	KI				CsI			
n_t	a	b	$(K^+)_y$	$(I^-)_z$	a	b	$(Cs^+)_y$	$(I^-)_z$
0.00	3.66	3.31	2.568	2.613	3.92	3.50	2.804	2.746
0.02	3.69	3.32	2.602	2.610	3.93	3.54	2.817	2.742
0.08	3.78	3.36	2.735	2.609	3.93	3.59	2.841	2.713
0.20	3.92	3.45	2.948	2.580	3.98	3.71	2.943	2.684
n_t(opt)[a]	3.97	3.54	3.042	2.551	4.04	3.73	3.041	2.657

[a] n_t(opt)=0.278 for KI and n_t(opt)=0.285 for CsI.

transfer is different from that of partial covalent binding between the ions and nanotube carbon because in the latter some of the electrons occupy molecular orbitals containing contributions from both ion and carbon atomic orbitals. By contrast, the mechanism described by the relations (2.6)–(2.8) involves no mixing between ion and wall orbitals but is characterized by the transfer of electrons from orbitals located entirely on the crystal to ones located entirely on the nanotube. The very small values of 0.00053 and 0.00087 a.u. for I_A^{ov} in KI and CsI, respectively, show that any electron transfer induced reduction of this energy is not the cause or even a significant contributor to the electron transfer process. This provides further evidence justifying the neglect of the distance dependence of I_A^{ov} needed to generate the second of the relations (2.7) from the first.

For each of the encapsulated KI and CsI crystals, the separations a and b predicted for that value of the charge transfer minimizing the energy (2.8), and presented in the fourth numerical row of Table III, are in excellent agreement with experiment. The first three columns of results for KI and CsI in Table IV show how the structural predictions change with increasing charge transfer. For zero charge transfer, both the a and b values are significantly underestimated even though a is predicted to be larger than the bulk R_e. The electrostatic interaction between the nanotube and crystal, that is, zero in the absence of charge transfer, necessarily becomes increasingly attractive as n is made larger thereby enhancing the magnitude of the opposite charges on the crystal and wall. The larger a values predicted on augmenting n are thus seen to originate from the increased crystal-wall electrostatic attractions. Furthermore, the results in Table IV show that the predicted b values also increase as n is made larger. These increases do not invalidate the arguments presented in Sec. III B 1 where it was explained why the prediction of increased a values resulting from reducing the ion-wall short-range repulsions necessarily yielded smaller values for b. The new factor in descending the columns in Table IV is that the removal of anion negative charge, corresponding to increasing n, reduces the large cation-anion electrostatic attractions which reduction must tend to increase b. It should not be regarded as surprising that the reduction in the magnitude of the largest energy term, namely, the point charge Madelung binding of the crystal, outweighs the more subtle effects described in Sec. III B 1. The two results for each crystal that, first, there is only one value of n which simultaneously reproduces both the experimental a and b values and, second, that this value is indeed the one yielding the lowest total energy globally provide extremely strong evidence that the present calculations have revealed the essential features determining the structures of the nanocrystals.

2. Spectroscopic probe of charge transfer

It has been established experimentally[59] that the frequency of one of the vibrational modes of a carbon nanotube is shifted by encapsulation of KI. Empty nanotubes to which known and independently determined quantities of charge were transferred also exhibit shifts in the frequency of the same vibrational mode.[60–67] These observations, coupled with the shift,[59] provide independent information concerning any exchange of charge when a nanotube encapsulates a crystal. The relevant nanotube vibration measured by Raman spectroscopy is the G or high energy mode (HEM) occurring at a frequency (ω) 1593 cm^{-1} in an empty nanotube. Encapsulation of KI has been observed[59] to induce a shift ($\Delta\omega$) in this mode of +2 cm^{-1}.

Direct information concerning the shift produced by the addition of electrons to nanotubes is provided by experimental measurements[62–64] of $\Delta\omega$ as a function of the measured weight of potassium metal added to nanotube bundles. Although the potassium nuclei do not enter individual nanotubes but become intercalated between the different tubes, these measurements yield directly $\Delta\omega$ as a function of added numbers of electrons per carbon because it is known[61,67–69] that each K atom donates its 4s electron to a nanotube. Thus the potassium/carbon ratio shown both in Fig. 2 of Ref. 62 and Fig. 1 of Ref. 63 is precisely the quantity designated here as nf. As nf initially increases from zero, ω decreases to produce a $\Delta\omega$ value of −1.2 cm^{-1} for nf=0.004. Further increase of nf causes ω to increase so that $\Delta\omega$ has become positive at 2–3 cm^{-1} for nf in the range 0.007–0.013. Further increase of nf causes ω to decrease monotonically until $\Delta\omega$ has become −8 cm^{-1} for the largest (0.04) value of nf accessible in the experiments.[62,63] Entirely independent experiments[64] yielded a precisely similar nonmonotonic dependence of $\Delta\omega$ on nf. Although $\Delta\omega$ varies nonmonotonically with nf, it has been established[62] by conduction electron spin resonance that nf does increase monotonically with the potassium doping level. Two other studies[61,65] reported negative $\Delta\omega$ for larger charge transfers but did not present a detailed examination for the smaller nf values showing non-

monotonically varying and sometimes positive $\Delta\omega$.[62–64] The experimental data in both Fig. 2 of Ref. 62 and Fig. 1 of Ref. 63 show that a measured $\Delta\omega$ of 2 cm^{-1} for the nanotubes encapsulating KI corresponds to an nf value in the range from 0.009 to 0.013. Since there are 28 (f^{-1}) carbon atoms per iodine nucleus, the prediction from our structural calculations that 0.278 electrons are transferred from each anion corresponds to an nf value of 0.0099. This result lies within the range consistent with the observed $\Delta\omega$, thus providing additional evidence for the reliability of the present predictions for the charge transfer.

The experimental measurements[62–64] on the potassium-nanotube intercalates show that the Raman frequency shift $\Delta\omega$ of 2 cm^{-1} measured[59] for nanotubes encapsulating KI is consistent with a transfer of between 0.009 and 0.013 electrons to each wall carbon atom. However, $\Delta\omega$ values have also been measured[65–67] as a function of the number of electrons electrochemically transferred from known weights of nonintercalated bundles of empty nanotubes. Increasing nanotube ionization caused $\Delta\omega$ to increase linearly by 250 cm^{-1} per electron withdrawn from each carbon atom.[65] Thus, the 2 cm^{-1} $\Delta\omega$ measured for the encapsulated KI system is also consistent with the ionization of 0.008 electrons from each carbon as well as with the transfer of 0.009–0.013 electrons to each such atom. However, the previous conclusion[59] that 0.007 electrons are transferred from the nanotube to the encapsulated KI was not derived by comparing the 2 cm^{-1} $\Delta\omega$ with the values directly measured in the experiments[60–67] where the nanotube charges were independently determined. It was instead inferred indirectly from a theoretical equation[66,67] linking $\Delta\omega/\omega$ to the nanotube strain in which the latter was related to the charge transfer. This equation states that $\Delta\omega/\omega$ equals $-2\gamma\varepsilon_{zz}$. Here, γ is a Grunneisen parameter and ε_{zz} is the strain that is the deviation of the carbon-carbon bond length from its equilibrium value in an electrically neutral nanotube. It was assumed[59] that γ was very close to unity in accordance with similar suggestions[67] made for related graphite intercalates. There is extensive experimental evidence[68–72] that ionization of electrons from graphite induces a negative ε_{zz} and that electron transfer to graphite causes ε_{zz} to increase. It was concluded,[59] by invoking the equality between $\Delta\omega/\omega$ and $-2\gamma\varepsilon_{zz}$, that observation of a positive $\Delta\omega$ implied a negative strain and hence that electrons had been transferred from the nanotube to the encapsulated KI. However, the experimental demonstrations[62–64] that positive $\Delta\omega$ can arise, not only from nanotube ionization but also from small amounts of electron transfer to the nanotube, show that the two stage argument[59] used to deduce nanotube ionization is not conclusive.

The above discussion shows that the two-step argument[59] used to infer nanotube ionization is invalidated by the experimental observation[62–64] that small quantities of electron transfer to nanotubes can also generate a positive $\Delta\omega$ value of 2 cm^{-1}. Currently there is probably insufficient evidence to locate the precise point at which the argument of Ref. 59 fails. Although a detailed discussion lies outside the scope of the present paper, a brief preliminary examination is of interest. It is our opinion that there is little reason to doubt the experimental evidence[68–70] that transfer of electrons to nanotubes lengthens the C–C bonds, corresponding to positive ε_{zz}. This can be understood because antibonding bands become partially filled with, furthermore, the additional electrons causing the magnitude of the negative resonance integral (β) to decrease.[73] The experimental evidence[70–72] that nanotube ionization contracts the C–C bonds would also seem to be incontrovertible. Here, the suggested theoretical explanation[73] is more subtle in that the bond length increase, which might be expected on withdrawing electrons from bonding bands, is more than offset by the positive charges thereby acquired by each carbon atom enhancing the magnitude of the resonance integral. It is well known that a longer bond normally implies a weaker bond with a smaller force constant and hence reduced vibration frequency as is necessary implied by equating $\Delta\omega/\omega$ to $-2\gamma\varepsilon_{zz}$ with positive γ close to unity. However, in the following model example, a small modification to a bond, causing it to expand and weaken, actually increases the force constant as opposed to reducing it as predicted by the above equality. Consider either a diatomic molecule or a bond in a polyatomic molecule whose energy $V(y)$ is given by $(1/2)ky^2$ for small displacements $y(=r-r_e)$ of the internuclear separation r from its equilibrium (r_e), the force constant thus being k. The addition of a small charge q to both atoms changes $V(y)$ to $(1/2)ky^2+q^2/(y+r_e)$ so that the new equilibrium separation (y_{ne}) is given by $ky_{ne}-q^2/(y_{ne}+r_e)^2=0$. This predicts a longer bond ($y_{ne}>0$). Even though the energy at the new equilibrium separation (r_e+y_{ne}) is predicted to be greater than zero, thus generating a longer bond with a smaller binding energy, the new force constant, $[d^2V(y)/dy^2]_{y=y_{ne}}=k+2q^2/(y_{ne}+r_e)^3$, is greater than the old value of k. Although we recognize that binding between adjacent carbon atoms in partially charged nanotubes will involve factors not described by this simple example, the demonstrated existence of a physically reasonable model in which bond lengthening is accompanied by an increased, rather than by a lowered, force constant shows that $\Delta\omega/\omega$ does not necessarily equal $-2\gamma\varepsilon_{zz}$ with positive γ close to unity.

The only reliable method of inferring the degree of charge transfer from the observed encapsulation induced +2 cm^{-1} shift[59] in the G band is by comparison with the results of those experiments[62–67] in which $\Delta\omega$ was measured as a function of known charge transfer. Thus, in the absence of any further independent arguments or experiments, it can only be concluded either that 0.008 electrons are ionized from each carbon atom or that each such atom gains between 0.009 and 0.013 electrons. However, without considering the results of the structural predictions presented in the present paper, the idea that 0.008 electrons are transferred away from each nanotube carbon to the encapsulated crystal can be rejected. Such a transfer would imply that each stoichiometric KI unit acquired 0.22 electrons. The charge could hardly be transferred to the iodide ion because, apart from already carrying a negative charge, this has a closed shell electronic structure having no vacant orbitals of low energy suitable for accommodating any further electrons. Furthermore two independent arguments show that this charge could not be accommodated on the K^+ ions. First, there is abundant evidence[61,68–70] that, even for potassium to carbon ratios up

to as high as 1/8, such as that occurring in potassium-graphite intercalates, each metal atom donates entirely its 4*s* electron to the graphite. This makes it very hard to believe that each potassium-based species retains as much a 0.22 of an electron in the encapsulated nanotubes where potassium/carbon ratios are much smaller. Second, any electron located in the 4*s* orbital of a K^+ ion in a KI ionic crystal would be unbound because, although a free cation can bind an extra electron with an energy[74] of 4.34 eV, in the nanocrystal any such electron would experience an additional destabilizing potential of $[M_T(a/b)]/b$ originating from the electrostatic field generated by the other ions as described in full detail in the next section. Since $M_T(a/b)$ is 1.5113 for KI, a potassium 4*s* electron would experience a destabilization of 6.22 eV thus causing it to be unbound by 1.88 eV. Though such a destabilization would not arise for the graphite intercalates, even in these materials the potassium atoms are fully ionized. Since one cannot reject the arguments that 0.008 electrons are not transferred from each nanotube carbon atom, the only conclusion that can be drawn from the observed encapsulation induced 2 cm^{-1} shift[59] in the frequency of the *G* mode is that each carbon atom gains between 0.009 and 0.013 electrons from the encapsulated KI.

3. Single anion description

An essentially single anion model for probing the charge transfer at fixed nuclear geometry, as defined solely by the *a* and *b* distances, yields further insights into the electron transfer process, three facets being very clearly and directly revealed. In this model, the only interspecies effect considered is that of the charge partially transferred to the wall ceasing to feel the environmental potential experienced by an anion electron in the crystal.

The in-crystal environmental potential experienced by an anion electron consists, in addition to the small overlap dependent term, contributing energies proportional to I_A^{ov} in the OHSMFS model[11] as described in Sec. II C, the much larger electrostatic energy. If the electrostatic potential generated by all other ions in the crystal treated as point charges is expanded in a series in which spherical harmonics are used to describe its angular variation, it is a purely mathematical result that only the spherically symmetric term affects the energy and electron density of a closed shell ion if it is assumed that this density remains spherically symmetric.[10] This potential, the first term in the OHSMFS Hamiltonian, is a constant attraction for distances r_a of an anion electron from its nucleus up to the closest cation-anion separation *R* after which it becomes less negative while undergoing smaller oscillations associated with anion-ion separations greater than the closest distances.[10,11,16] Thus for the rocksalt structured bulk crystal, this first contribution to the OHSMFS potential is, for $r_a \leqslant R$, a constant stabilizing Madelung term $-M/R$ with *M* the Madelung constant.

For a nanocrystal in which each of the (2×2) planes is square, not inconsistent with the experimental data, the electrostatic potential energy experienced by an anion electron at distances r_a less than the closest cation-anion separation is constant having the value $-M_T(x)/b$ equal to the Madelung potential determining the electrostatic contribution to the crystal cohesive energy. Here $x=a/b$ with $M_T(x)$ being given by[57]

$$M_T(x) = 2\ln 2 + M_b(x). \tag{3.1}$$

In this equation, the first contribution arises from electrostatic potential energy of $-2\ln 2/b$ generated by all the other ions in the same chain while the contribution to $M_T(x)$ from all other chains of ions is given by $-M_b(x)/b$ with the Madelung function $M_b(x)$ being defined by Eq. (11) of Ref. 57. Since the large majority of each anion electron density arises at distances r_a smaller than the distance to the closest cations, the expectation value of the first (electrostatic) term in the OHSMFS potential will be given by $-M_T(x)/b$. This shows that, for an anion electron in (2×2) nanocrystal having four cation neighbors, its effective one-electron energy I_A including the interaction with the environment generated by the other ions in the nanocrystal is given by

$$I_A = I_A^{ne} - M_T(x)/b + 4I_A^{ov}. \tag{3.2}$$

Considering only the last two terms of Eq. (3.2) in addition to the purely one-center terms (2.3), which already include I_A^{ne}, shows that the total energy of a system in which *n* electrons are transferred from just one anion to f^{-1} wall carbon to be given by

$$E_T(n) = (4-n)I_A + (1/2)(4-n)(3-n)F_A + f^{-1}[(1+nf)I_W + (1/2)(1+nf)nfF_W], \tag{3.3}$$

which differs from Eq. (2.3) only in that I_A^{ne} has been replaced by I_A.

The result (3.3) will only provide a useful description of the system in which *n* electrons are transferred from every nanocrystal anion if the sum of three effects arising from the partial ionization of neighboring ions is significantly smaller than the sum of the last two terms in Eq. (3.2). These effects are the attraction to the positively charged crystal of the electrons transferred to the wall, the mutual repulsion between these wall electrons on different atoms, and the more negative value of the effective one-electron energy (I_A) for an anion close to another partially ionized anion even when I_A^{ne} remains unchanged. The first two of these effects are identical to the first of the four interspecies interactions introduced in Sec. II C and automatically included in Eq. (2.6) through the computation of $U^{GULP}(\boldsymbol{r}_X;n)$. The third of the factors listed in Sec. II C as automatically included in the computation of $U^{GULP}(\boldsymbol{r}_X;n)$, the reduction in the Madelung binding of the partially ionized nanocrystal, encompasses both the term $-nM_T(x)/b$ introduced into Eq. (3.3) through Eq. (3.2) and the effect omitted from Eq. (3.3), that of the more negative I_A value for anions close to partially ionized anions. The quantity $\Delta E_{int}^{GULP}(n)$ defined as a function of *n* by

$$\Delta E_{int}^{GULP}(n) = U^{GULP}(\boldsymbol{r}_{X_e};n) - U^{GULP}(\boldsymbol{r}_{X_e};0) \tag{3.4}$$

is the difference between the GULP energies predicted for nonzero and zero *n* with both terms evaluated for the same ion positions $\boldsymbol{r}_{X_e}$ that are optimal for the crystal with charge transfer specified by *n*. For all *n* values encompassing the range from zero to n_t for both KI and CsI, the computed

differences $\Delta E_{\mathrm{int}}^{\mathrm{GULP}}(n)$ were found to be essentially identical with those calculated as $nM_T(x)/b$ from which they usually differed by less than 1% and certainly by no more than a few percent provided that the latter were evaluated for the values of x and b corresponding to the equilibrium geometry as defined by the $\mathbf{r}_{X_e}$ in Eq. (3.4). This shows that loss of the Madelung binding of the ionized charge is the dominant multicenter interaction governing the charge transfer and that the sum of the three other interspecies terms presented after and not included in Eq. (3.3) is much smaller. This result validates using the approximate relation Eq. (3.3) to investigate the charge transfer at fixed nuclear geometry. It should be noted, however, that the energy (3.3) is not totally independent of this geometry because the value of I_A depends on b and x. Thus the quantity $nM_T(x)/b$ differs more significantly from the computed $\Delta E_{\mathrm{int}}^{\mathrm{GULP}}(n)$ values if the former is evaluated from a geometry differing from that used in Eq. (3.4). However, it can be seen that Eq. (3.3) does not include any energy differences between nanocrystals having square or diamond shaped (2×2) planes provided the nanocrystals have the same values of b and x. The energies $nM_T(x)/b$ were calculated assuming square (2×2) planes while the $\Delta E_{\mathrm{int}}^{\mathrm{GULP}}(n)$ values were derived from the fully optimized computations yielding diamond shaped planes, as discussed in the next section. The similarity of these two values for each n shows that the energy differences arising from the distortions of the planes from square to diamond are small provided a is kept constant.

The energy $E_T(n)$ (3.3) is not referred to the same zero of energy as that in Eq. (2.6) because, in the former, the energy $E_T(0)$ is not subtracted. However, since the latter is a constant, the number n_t of electrons actually transferred from each anion is that minimizing $E_T(n)$, being given by

$$n_t = [I_A + (7/2)F_A - I_W - F_W/2]/[F_A + fF_W]. \tag{3.5}$$

This result yields three predictions concerning n_t which do not depend on the values of the carbon energies I_W and F_W. First, there will be no charge transfer if the anion electrons are so strongly bound that the numerator of Eq. (3.5) is negative, this arising for large negative values of I_A. Second, the charge transfer in CsI is predicted to be greater than that in KI, because I_A^{ne} and F_A in CsI are so similar to those in KI that the difference between the I_A values of these two materials is dominated by the difference in the in-crystal electrostatic energies as expressed by the $M_T(x)/b$ term. Since the respective $M_T(x)$ values of 1.51131 and 1.52521 in KI and CsI evaluated from the experimental a and b distances are so close, the electrostatic binding energy of an anion electron will be lower in CsI than in KI because b is greater in the former. This causes the magnitude of the negative I_A in CsI to be smaller than that in KI, thus leading through Eq. (3.5) to a greater charge transfer in CsI crystal. The third deduction from Eq. (3.5) is that the charge transfer will be insensitive to the detailed structure and even dimensions of the encapsulating nanotube. This follows because the only nanotube parameter entering Eq. (3.5), the fraction f of the number of anions per carbon, is small thus causing the denominator to depend only weakly on f.

For KI and CsI, the RIP/RELCRION computations yielded values for F_A of 0.32889 and 0.33287 a.u. while the analysis presented in the Appendix yielded a value for F_W of 0.41254 a.u. Substitution of these values together with those already presented for I_A^{ne}, I_W, and $M_T(x)$ predicts that the charge transfers in KI and CsI are, respectively, 0.22 and 0.27 electrons per anion. The similarity between these values and those of 0.278 and 0.285 predicted from the more sophisticated approach based on Eq. (2.6) confirms that theory yielding Eq. (3.3) does indeed capture the essential physics of the charge transfer process. This ensures the validity of the insights into the charge transfer gleaned from Eq. (3.5) described above. The charge transfer predicted for CsI is not very dissimilar to that obtained for KI. The relation (3.5) shows that this similarity arises because here the environmental dependence enters entirely from the term $M_T(x)/b$ which has only a relatively weak dependence on b with the variation of $M_T(x)$ being even weaker. This shows that the charge transfer depends only weakly on structure but that the structural predictions are much more sensitive to the charge transferred, as shown by the results presented in Table IV.

4. Charge transfer generated structural evolution

The main focus of this paper has been elucidating and explaining the factors determining the a and b separations because these are the quantities which have so far been measured. Nevertheless it is of interest to examine the detailed shapes of the (2×2) planes because there are no symmetry reasons requiring these to be exactly square. Since the interaction energy of two cations is not exactly the same as that of two iodide ions, it should be expected that each plane will be slightly distorted from a square shape even in the absence of charge transfer $(n=0)$. The results presented in Table IV do indeed show that each plane is diamond shaped even for $n=0$.

The transfer of negative charge to the wall will introduce an electrostatic attraction between the cations and the wall explaining why (Table IV) the cation-cation distance $2(\mathrm{K}^+)_y$ increases with increasing n. Enhancing charge transfer generates an increasing electrostatic repulsion between the wall and the iodide ions which progressively reduces the separation $2(\mathrm{I}^-)_z$ between the two iodide ions. These effects are revealed by the computations based on the more exact theory provided by Eq. (2.6) even though they are not captured by the more approximate single anion theory presented in the Sec. III C 3, this latter being introduced to gain physical insight into the charge transfer but not to make structural predictions. For both KI and CsI at their experimental equilibrium geometries, as predicted for the case of optimal charge transfer $(n=n_t)$, the magnitudes of these two electrostatic ion-wall interactions are sufficiently large that the separation between the two cations in any plane is greater than that of a pair of anions. However, the relative smallness of the deviation from square explains why there is currently no experimental information about the geometry beyond the a and b values.

IV. CONCLUSIONS

The structures and electronic charge distributions of nanocrystalline KI and CsI containing four ions in cross section when encapsulated in a SWNT have been investigated theoretically. Not only do our predictions for the structures of the nanocrystals agree with experiment but we have also shown that such encapsulation causes a significant transfer, of slightly more than 1/4 of an electron per anion, to the wall carbon atoms. Such transfers correspond to a gain of about 0.01 electrons by each such atom. This prediction is supported by independent evidence from Raman spectroscopy showing that encapsulation of KI increases the frequency of a nanotube vibrational mode by 2 cm^{-1}. Comparison of this result, with the corresponding frequency increases for nanotubes to which independently known numbers of electrons were transferred, shows that a 2 cm^{-1} shift corresponds to a gain in the range from 0.009 to 0.013 electrons per carbon atom encompassing our prediction. These transfers of charge from the encapsulated crystals to the nanotube wall suggest that the electrical properties of the nanotube could be significantly modified.

In the computation of the short-range repulsion between an ion and the wall carbons using a local DFT approach, the semiconducting or metallic nature of the tube is the source of the large value for the effective number of electrons entering the calculation of the exchange interaction. It has been shown that both this effect and the charge transfer play a crucial role in determining the structures of the encapsulated ionic crystals. This contrasts the minimal role played by multipoles on the wall carbon.

The conclusions that both the electronic properties of the empty nanotubes and the charge transfer in the encapsulated materials, here elucidated for KI and CsI, play an important role in determining their structures and electrical properties is likely to apply to the majority, if not all, such guest-host systems. Both these effects will therefore need to be considered in order to understand the full details of the experimentally observed structures of both encapsulated (2×2) RbI (Ref. 75) and of KI and CsI (3×3) nanocrystals[75,76] encapsulated in larger carbon nanotubes. It is most unlikely that these effects, especially charge transfer, will prove to be any less significant for a variety, much more extensive than the alkali halides, of already prepared[77] encapsulated nanocrystalline metal salts. Structural predictions also have been derived,[78,79] using semiempirically determined short-range repulsions, for a wide variety of crystals, treated on a fully ionic basis, encapsulated in numerous nanotubes, a level of treatment comparable with the Born model description[57] of the alkali halide nanocrystals. The resulting predictions are valuable in suggesting the existence of a very rich variety of different structures, thereby motivating the experimental search for such materials, the vast majority of which have not so far been observed. Since these predictions did not consider the possibility of charge transfer, the present results for encapsulated KI and CsI suggest that this would need to be considered in any detailed comparison with experimental data, which may subsequently become available.

Good agreement between the predicted and experimental structures can only be achieved both by introducing a realistic description of the anion to wall charge transfer and by recognition of the large value of the effective number of electrons influencing the exchange interaction in the DFT description of the short-range ion-wall interactions. It should be emphasized that, for each nanocrystal, the only value for the charge transfer predicting the experimentally observed structure is that minimizing the total energy. Furthermore, the generated structures changed in rather different yet physically understandable ways on changing both the charge transfer and ion-wall interactions with correct predictions obtained only with the right charge transfer and description of the ion-wall interactions shown to be physically correct by the investigation[14] of the adsorption of noble gases by graphite.

Although the charge transfer predicted by minimizing the energy depends only weakly on the assumed nuclear geometry, the predicted structures are sensitive to the charge transfer. This charge transfer is predicted to cause the separations between the two cations in each (2×2) plane to be greater than those between the two anions causing each plane to be diamond shaped. Although the accuracy of the present experimental data[1,4] does not allow the case of entirely square planes to be distinguished from those exhibiting the small diamond like distortions predicted here, it is to be hoped that future more accurate experiments might discriminate between these two possibilities.

ACKNOWLEDGMENTS

The authors thank Professor B. F. G. Johnson, Professor A. I. Kirkland, and Professor J. Harding, for useful discussions. They also thank The Newton Trust (Cambridge University) and The Leverhulme Trust Foundation for financial support.

APPENDIX

In the standard notation the repulsion, denoted F_W in the main text, between two carbon electrons in occupying the same $p\text{-}\pi(p_z)$ atomic orbital equals the integral $\langle p_z(1)p_z(2)|r_{12}^{-1}|p_z(1)p_z(2)\rangle$. This integral is expressed in terms of the Slater integrals $F^{(0)}$ and $F^{(2)}$ by[80]

$$F_W = F^{(0)} + (4/25)F^{(2)}. \tag{A1}$$

The one-electron energy I_W, consisting of the electron kinetic energy, attraction to the nucleus and repulsion with two $1s$ electrons, one $2s$ electron, and one electron in each of the $2p_x$ and $2p_y$ orbitals was calculated from the optimal level wavefunction[81] computed for the ^1S state of the ground configuration of the carbon atom using the Oxford Dirac–Fock program.[82] After introducing the Cowan DFT estimate of the contribution from electron correlation, $F^{(0)}$ was predicted to be 0.41789 a.u. Since it was not possible to perform a similar calculation of the correlation contribution to $F^{(2)}$, this entire quantity was evaluated by analyzing experimental data.

The valence ($2p$ electron) energies of the following states of the ground configurations of the cationic, neutral, and anionic states of carbon are given by[80]

$$E(C^+) = I_{2p},$$

$$E(C\ ^1S) = 2I_{2p} + F^{(0)} + (2/5)F^{(2)},$$

$$E(C\ ^1D) = 2I_{2p} + F^{(0)} + (1/25)F^{(2)}, \quad \text{(A2)}$$

$$E(C\ ^3P) = 2I_{2p} + F^{(0)} - (1/5)F^{(2)},$$

$$E(C^-\ ^2D) = 3I_{2p} + 3F^{(0)} - (6/25)F^{(2)},$$

$$E(C^{-4}S) = 3I_{2p} + 3F^{(0)} - (3/5)F^{(2)},$$

where $I_{2p} \neq I_W$ is, for a single electron in the $2p$ orbital the sum of its kinetic energy, attraction to the nucleus and repulsion with the four s electrons. Choosing pairs of states belonging to the same state of ionization but with the smallest spin multiplicity difference, two values for $F^{(2)}$ can be derived by equating the two differences $E(C^-\ ^2D) - E(C^-\ ^4S)$ and $E(C\ ^1S) - E(C\ ^1D)$ to the experimental differences of 0.045165 a.u. (Ref. 83) and 0.05219 a.u.[84] This yields $F^{(2)}$ values of 0.12546 and 0.14498 a.u., respectively. Equating the experimental ionization potential for $C(^3P)$ of 0.41379 a.u.[74] to the result for $E(C^+) - E(C\ ^3P)$ while also equating the experimental electron affinity of 0.04641 a.u. to[83] $E(C^-\ ^2D) - E(C\ ^3P)$ and solving the two resulting simultaneous equations yields $F^{(0)}$ values of 0.39247 and 0.39637 a.u. when $F^{(2)}$ is taken to be 0.12546 and 0.14498 a.u., respectively. The first value, used for all the results reported in the main text, yields predictions of 0.22 and 0.27 for n_t for KI and CsI in Sec. III C 3.

Invoking the second $F^{(2)}$ result of 0.14498 a.u. yields a value of 0.41957 a.u. for F_W with it then being predicted using Eq. (3.5) that n_t are 0.21 and 0.26 for KI and CsI, respectively. These results are essentially unchanged from those reported in the main text. Combination of the first $F^{(2)}$ result with the *ab initio* $F^{(0)}$ yields an F_W of 0.43796 a.u. thus predicting through Eq. (3.5) the slightly smaller charge transfers of 0.18 and 0.24 for KI and CsI, respectively.

All three sets of predictions for n_t are sufficiently similar that it can be concluded that both the more exact theory leading to Eqs. (2.6)–(2.8) and the "single anion" result (3.5) do indeed capture the essential physics of the anion to wall charge transfer.

[1] J. Sloan, M. C. Novotny, S. R. Bailey *et al.*, Chem. Phys. Lett. **329**, 61 (2000).
[2] M. Ahtee, Ann. Acad. Sci. Fenn., Ser. A6 **313**, 1 (1969).
[3] M. Blackman and I. H. Khan, Proc. Phys. Soc. **77**, 471 (1961).
[4] J. Sloan, A. I. Kirkland, J. L. Hutchison, and M. L. H. Green, C. R. Phys. **4**, 1063 (2003).
[5] M. Wilson and P. A. Madden, J. Am. Chem. Soc. **123**, 2101 (2001).
[6] M. Wilson, J. Chem. Phys. **116**, 3027 (2002).
[7] G. Brown, S. R. Bailey, M. Novotny, R. Carter, E. Flahaut, K. S. Coleman, J. L. Hutchison, M. H. L. Green, and J. Sloan, Appl. Phys. A: Mater. Sci. Process. **76**, 457 (2003).
[8] C. Yam, C. Ma, X. Wang, and G. Chen, Appl. Phys. Lett. **85**, 4484 (2004).
[9] E. L. Sceats, J. C. Green, and S. Reich, Phys. Rev. B **73**, 125441 (2006).
[10] N. C. Pyper, Philos. Trans. R. Soc. London, Ser. A **320**, 107 (1986).
[11] N. C. Pyper, Philos. Trans. R. Soc. London, Ser. A **352**, 89 (1995).
[12] N. C. Pyper, J. Phys.: Condens. Matter **7**, 9127 (1995).
[13] N. C. Pyper, J. Chem. Phys. **118**, 2308 (2003).
[14] E. Bichoutskaia and N. C. Pyper, J. Chem. Phys. **128**, 024709 (2008).
[15] M. P. Housden and N. C. Pyper, J. Phys.: Condens. Matter **20**, 085222 (2008).
[16] N. C. Pyper, Adv. in Solid-State Chem. **2**, 223 (1991).
[17] P. A. Madden and M. Wilson, Chem. Soc. Rev. **25**, 339 (1996).
[18] J. H. Harding, P. J. D. Lindan, and N. C. Pyper, J. Phys.: Condens. Matter **6**, 6485 (1994).
[19] N. C. Pyper, A. I. Kirkland, and J. H. Harding, J. Phys.: Condens. Matter **18**, 683 (2006).
[20] N. C. Pyper and P. Popelier, J. Phys.: Condens. Matter **7**, 5013 (1995).
[21] N. C. Pyper, J. Phys.: Condens. Matter **8**, 5509 (1996).
[22] A. Tkatchenko and O. A. von Lilienfeld, Phys. Rev. B **73**, 153406 (2006).
[23] J. D. Gale and A. L. Rohl, Mol. Simul. **29**, 291 (2003).
[24] A. Vernon and W. A. Steele, Langmuir **8**, 155 (1991).
[25] J. C. Ma and D. A. Doughty, Chem. Rev. (Washington, D.C.) **97**, 1303 (1997).
[26] D. G. Dick and A. W. Overhauser, Phys. Rev. **112**, 90 (1958).
[27] M. P. Housden and N. C. Pyper, Mol. Phys. **105**, 2353 (2007).
[28] N. Jacobi and Gy. Csanak, Chem. Phys. Lett. **30**, 367 (1975).
[29] J. C. Slater and J. G. Kirkwood, Phys. Rev. **37**, 682 (1931).
[30] P. W. Fowler and N. C. Pyper, Proc. R. Soc. London, Ser. A **398**, 377 (1985).
[31] P. W. Fowler, P. J. Knowles, and N. C. Pyper, Mol. Phys. **56**, 83 (1985).
[32] P. W. Fowler and P. A. Madden, Mol. Phys. **49**, 913 (1983).
[33] P. W. Fowler and P. A. Madden, Phys. Rev. B **29**, 1035 (1984).
[34] P. W. Fowler and P. A. Madden, J. Phys. Chem. **89**, 258 (1985).
[35] A. D. Crowell, Surf. Sci. Lett. **111**, L667 (1981).
[36] W. E. Carlos and M. W. Cole, Surf. Sci. **91**, 339 (1980).
[37] G. Vidali, M. W. Cole, and J. R. Klein, Phys. Rev. B **28**, 3064 (1983).
[38] G. Starkschall and R. G. Gordon, J. Chem. Phys. **56**, 2801 (1972).
[39] P. W. Fowler and N. C. Pyper, Mol. Phys. **59**, 317 (1986).
[40] H. Margenau and N. R. Kestner, *Theory of Intermolecular Forces*, 1st ed. (Pergamon, New York, 1969), Chap. 9, p. 292.
[41] H. J. Werner and W. Meyer, Phys. Rev. A **13**, 13 (1976).
[42] *CRC Handbook of Physics and Chemistry*, 86th ed., edited by R. C. Weast (CRC, Boca Raton, FL, 2003).
[43] J. N. Wilson and R. M. Curtiss, J. Phys. Chem. **74**, 187 (1970).
[44] M. J. L. Sangster and R. M. Atwood, J. Phys. C **11**, 1541 (1978).
[45] C. P. Wood and N. C. Pyper, Philos. Trans. R. Soc. London, Ser. A **320**, 71 (1986).
[46] N. C. Pyper, Chem. Phys. Lett. **220**, 70 (1994).
[47] R. G. Gordon and Y. S. Kim, J. Chem. Phys. **56**, 3122 (1972).
[48] R. D. Cowan, Phys. Rev. **163**, 54 (1967).
[49] H. S. W. Massey and D. W. Sida, Philos. Mag. **46**, 190 (1955).
[50] A. I. M. Rae, Chem. Phys. Lett. **18**, 574 (1973).
[51] A. I. M. Rae, Mol. Phys. **29**, 467 (1975).
[52] J. Lloyd and D. Pugh, J. Chem. Soc., Faraday Trans. 2 **73**, 234 (1977).
[53] M. J. Clugston and N. C. Pyper, Chem. Phys. Lett. **63**, 549 (1979).
[54] C. P. Wood and N. C. Pyper, Mol. Phys. **43**, 1371 (1981).
[55] N. C. Pyper and I. P. Grant, Proc. R. Soc. London, Ser. A **339**, 525 (1978).
[56] R. G. Parr, *Aspects of Density Functional Theory in Local Density Approximations in Quantum Chemistry and Solid State Physics*, edited by J. P. Dahl and J. Avery (Plenum, New York, 1984), pp. 21–31.
[57] E. Bichoutskaia and N. C. Pyper, J. Phys. Chem. B **119**, 5936 (2006).
[58] J. E. Lennard-Jones and B. M. Dent, Trans. Faraday Soc. **24**, 92 (1928).
[59] A. Ilie, J. S. Bendall, D. Roy, E. Philip, and M. L. H. Green, J. Phys. Chem. B **110**, 13848 (2006).
[60] R. S. Lee, H. J. Kim, J. E. Fischer, A. Thess, and R. E. Smalley, Nature (London) **388**, 255 (1997).
[61] A. M. Rao, P. C. Eklund, S. Bandow, A. Thess, and R. E. Smalley, Nature (London) **388**, 257 (1997).
[62] A. S. Claye, N. M. Nemes, A. Janossy, and J. E. Fischer, Phys. Rev. B **62**, R4845 (2000).
[63] A. Claye, S. Rahman, J. E. Fischer, A. Sirenko, G. U. Sumanasekera, and P. C. Eklund, Chem. Phys. Lett. **333**, 16 (2001).
[64] Y. Iwasa, H. Fudou, T. Yatsu, T. Mitani, Y. Achiba, and H. Kataura, APS Meeting Abstract, 2000 (unpublished).
[65] L. Kavan, P. Rapta, L. Dunsch, M. J. Bronikowski, P. Willis, and R. E. Smalley, J. Phys. Chem. B **105**, 10764 (2001).
[66] M. Stoll, P. M. Rafailov, W. Frenzel, and C. Thomsen, Chem. Phys. Lett. **375**, 625 (2003).
[67] P. M. Rafailov, M. Stol, and C. Thomsen, J. Phys. Chem. B **108**, 19241 (2004).

[68] D. E. Nixon and G. S. Parry, J. Phys. C **2**, 1732 (1969).
[69] P. C. Eklund, G. Dresselhaus, M. S. Dresselhaus, and J. E. Fischer, Phys. Rev. B **16**, 3330 (1977).
[70] C. T. Chan, W. A. Kamitakahara, and K. M. Ho, Phys. Rev. Lett. **58**, 1528 (1987).
[71] R. S. Markiewicz, R. S. Kasper, and L. V. Interrante, Synth. Met. **2**, 363 (1980).
[72] W. A. Kamitakahara, J. L. Zaretsky, and P. C. Eklund, Synth. Met. **12**, 301 (1985).
[73] L. Pietronero and S. Strassler, Phys. Rev. Lett. **47**, 593 (1981).
[74] C. E. Moore, *Atomic Ionization Potentials and Ionization Limits Derived From the Analysis of Optical Spectra*, Natl. Bur. Stand. Ref. Data Ser., Natl. Bur. Stand. (U.S.) Circ. No. 34 (U.S. GPO, Washington D.C., 1971).
[75] J. Sloan, A. I. Kirkland, J. L. Hutchison, and M. L. H. Green, C. R. Phys. **4**, 1063 (2003).
[76] R. R. Meyer, J. Sloan, R. E. Dunin-Borkowski, A. I. Kirkland, M. C. Novotny, S. R. Bailey, J. L. Hutchison, and M. L. H. Green, Science **289**, 1324 (2000).
[77] J. Sloan, A. I. Kirkland, J. L. Hutchison, and M. L. H. Green, Chem. Commun. (Cambridge) **2002**, 1319.
[78] M. Wilson, Chem. Phys. Lett. **397**, 340 (2004).
[79] M. Wilson, J. Chem. Phys. **124**, 124706 (2006).
[80] E. U. Condon and G. H. Shortley, *The Theory of Atomic Spectra* (Cambridge University Press, Cambridge, 1935).
[81] I. P. Grant, D. F. Mayers, and N. C. Pyper, J. Phys. B **9**, 2777 (1976).
[82] I. P. Grant, B. J. McKenzie, P. H. Norrington, D. F. Mayers, and N. C. Pyper, Comput. Phys. Commun. **21**, 207 (1980).
[83] B. M. Smirnov, *Negative Ions*, translated by S. Chomet and H. S. W. Massey (McGraw-Hill, 1982), Table. 1.10.
[84] C. E. Moore, *Atomic Energy Levels*, Natl. Bur. Stand. (U.S.) Circ. No. 467 (U.S. GPO, Washington D.C., 1949), Vol. 1.
[85] E. N. Lassettre, J. Chem. Phys. **43**, 4479 (1965).